

Visualizing weak ferromagnetic domains in multiferroic hexagonal ferrite thin filmWenbo Wang,¹ Julia A. Mundy,² Charles M. Brooks,³ Jarrett A. Moyer,⁴ Megan E. Holtz,² David A. Muller,^{2,5} Darrell G. Schlom,^{3,5} and Weida Wu^{1,*}¹*Department of Physics and Astronomy, Rutgers University, Piscataway, New Jersey 08854, USA*²*School of Applied and Engineering Physics, Cornell University, Ithaca, New York 14853, USA*³*Department of Materials Science and Engineering, Cornell University, Ithaca, New York 14853, USA*⁴*Department of Physics and Frederick Seitz Materials Research Laboratory, University of Illinois at Urbana-Champaign, Urbana, Illinois 61801, USA*⁵*Kavli Institute at Cornell for Nanoscale Science, Ithaca, New York 14853, USA*

(Received 20 January 2017; revised manuscript received 5 April 2017; published 26 April 2017)

We report cryogenic magnetic force microscopy (MFM) studies of a 200-nm-thick hexagonal (*h*) LuFeO₃ film grown by molecular-beam epitaxy on a (111)-oriented yttria-stabilized cubic-zirconia substrate. Labyrinthlike domains $\sim 1.8 \mu\text{m}$ in size were observed after zero-field cooling below the Néel temperature, $T_N \approx 147 \text{ K}$, where weak ferromagnetic order ($P6_3cm$) with a canted moment of $M_S \approx 0.02 \mu_B/\text{f.u.}$ exists. At 6 K, MFM images of the magnetization reversal process reveal a typical domain behavior of a pinning-dominated hard magnet. The pinning strength is substantially reduced at elevated temperature. The temperature dependence of the domain contrast demonstrates that our MFM is able to detect the domain contrast of magnets with tiny magnetic moments ($\sim 0.002 \mu_B/\text{f.u.}$). An upper limit of the linear magnetoelectric coefficient of *h*-LuFeO₃ ($\alpha_{zz} < 6 \text{ ps/m}$) is estimated by magnetoelectric force microscopy measurements.

DOI: [10.1103/PhysRevB.95.134443](https://doi.org/10.1103/PhysRevB.95.134443)**I. INTRODUCTION**

Multiferroic materials, which possess at least two ferroic properties among ferroelectricity, ferromagnetism, and ferroelasticity, are of great interest to condensed-matter physicists due to the possible giant cross couplings between these three order parameters [1–4]. The cross coupling between ferroelectric and ferromagnetic orderings gives rise to a large magnetoelectric (ME) effect, i.e., electric polarization induced by magnetic field or magnetization induced by electric field [5–7]. The ME effect has a wide range of applications in electric-field-controlled magnetic memories [8,9], magnetic field sensors [10,11], and tunable microwave filters [12,13]. Extensive studies have been carried out on transition-metal oxide multiferroics, such as BiFeO₃ [14–18], and hexagonal rare-earth manganites (*h*-RMnO₃, $R = \text{Y, Dy-Lu}$) [19–23]. Recently, the *h*-LuFeO₃ thin film, a member of hexagonal ferrites (*h*-RFeO₃, $R = \text{Y, Dy-Lu}$), has been claimed to be another multiferroic material, with potential ME coupling [24–30]. Similar to hexagonal manganites, hexagonal ferrites exhibit both ferroelectricity and antiferromagnetism. *h*-LuFeO₃ is, however, more appealing because of its weak ferromagnetic ground state with significant canted moment ($\sim 0.02 \mu_B/\text{f.u.}$) and its higher magnetic ordering temperature ($T_N \approx 147 \text{ K}$) [28], presumably due to the stronger exchange interaction between Fe³⁺ moments [31].

Unfortunately, the hexagonal phase of LuFeO₃ is unstable when synthesized in ambient condition. The stable polymorph of LuFeO₃ has the perovskite structure and is orthorhombic. There are two effective routes to stabilize the hexagonal polymorph of LuFeO₃. One route is chemical doping of either Mn onto the Fe site or Sc onto the Lu site in bulk crystals [32–35]. The other is the epitaxial growth of thin films of

the metastable phase on substrates with trigonal symmetry [36]. High-quality *h*-LuFeO₃ films have been synthesized by metal-organic chemical vapor deposition (MOCVD) [36], pulsed laser deposition (PLD) [27], and molecular-beam epitaxy (MBE) [28,30]. Stoichiometric LuFeO₃ films have a weak ferromagnetic ordering at $T_N \sim 147 \text{ K}$ [28]. The weak ferromagnetism comes from the canted moments of 120° ordered Fe³⁺ spins in the A₂ ($P6_3cm$) phase. More interestingly, recent theory predicts a linear magnetoelectric (ME) coupling in *h*-LuFeO₃ with $\alpha_{zz} \sim 0.16 \text{ ps/m}$ [31]. In the A₂ phase, the magnetoelectric coefficient is proportional to the product of the canted moment (\mathbf{M}_z) and the ferroelectric polarization (\mathbf{P}_z), i.e., $\alpha_{zz} \propto \mathbf{P}_z \cdot \mathbf{M}_z$ [23]. Thus, it is crucial to directly visualize the ferroelectric and weak ferromagnetic domains to understand ME coupling in *h*-LuFeO₃. Direct imaging, however, of the weak ferromagnetic domains is quite challenging because of the small canted moment ($0.02 \mu_B/\text{f.u.}$) [28].

In this paper, we report cryogenic magnetic force microscopy (MFM) studies on a ~ 200 -nm-thick *h*-LuFeO₃ film epitaxially grown on a (111)-oriented yttria-stabilized cubic-zirconia (YSZ) substrate. Labyrinthlike weak ferromagnetic domains with an average size of $\sim 1.8 \mu\text{m}$ were observed below $T_N \approx 147 \text{ K}$. The MFM results are in good agreement with the magnetization data. This suggests the local measurements by MFM are representative of bulk properties. The field-dependent MFM results exhibit a typical domain behavior of a hard ferromagnet with a strong pinning effect.

II. MATERIALS AND METHODS

The *h*-LuFeO₃ film was grown by oxide MBE in a Veeco GEN10 MBE system at a growth temperature of $\sim 800^\circ\text{C}$ as measured by optical pyrometry. Effusion cells were used to thermally evaporate lutetium and iron at elemental fluxes of $\sim 1 \times 10^{13} \text{ atoms}/(\text{cm}^2 \text{ s})$ onto $10 \times 10 \text{ mm}$ (111)-oriented

*Corresponding author: wdwu@physics.rutgers.edu

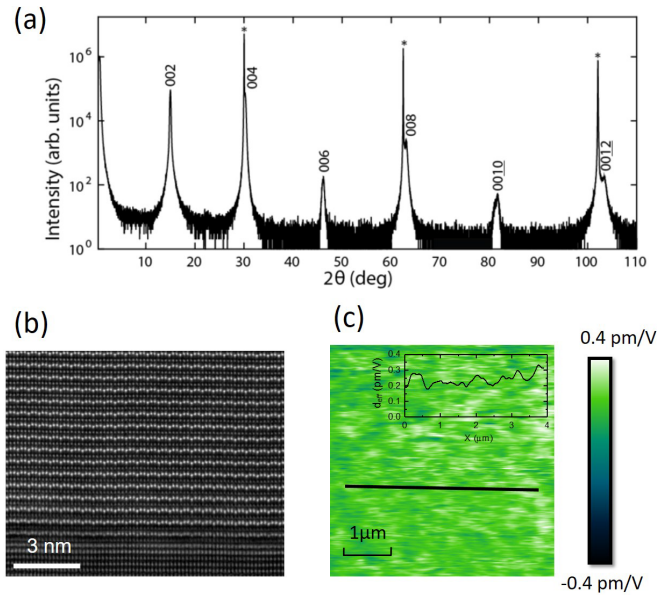


FIG. 1. (a) $\theta - 2\theta$ XRD data at room temperature, with h -LuFeO₃ 00 l reflections labeled accordingly; substrate peaks are denoted by (*). (b) HAADF-STEM image of the h -LuFeO₃/YSZ interface. The “up-up-down” pattern of the lutetium atoms observed in the film is consistent with a polar domain structure. (c) PFM image at room temperature without any image processing, which shows a spatially uniform and positive piezoelectric response. The inset shows the profile of PFM signals along the solid line in (c).

yttria-stabilized cubic-zirconia (YSZ) substrates. Oxidation of the incident lutetium and iron fluxes was provided by a mixture of oxygen and $\sim 10\%$ ozone supplied at a background partial pressure of 1×10^{-6} Torr. The x-ray diffraction (XRD) data taken on the 200-nm-thick h -LuFeO₃ film exhibits 00 l reflection peaks with even l , consistent with single phase $P6_3cm$ with (001) orientation, as shown in Fig. 1(a). The room-temperature ferroelectricity of h -LuFeO₃ was investigated by using high-angle annular dark-field scanning transmission electron microscopy (HAADF-STEM) [37]. A representative HAADF-STEM was shown in Fig. 1(b). The characteristic “up-up-down” pattern of the lutetium atoms indicates a monodomain structure with up polarization. This was also confirmed by a background-free piezoresponse force microscopy (PFM) measurement at ambient condition [38,39], which shows a positive piezoelectric response $d_{33} \approx 0.24$ pm/V over a $5 \mu\text{m}$ region [see Fig. 1(c)]. The MFM experiments were carried out in a homemade cryogenic atomic force microscope (AFM) using commercial piezoresistive cantilevers (spring constant $k \approx 3$ N/m, resonant frequency $f_0 \approx 42$ kHz). The homemade AFM is interfaced with a Nanonis SPM Controller and a commercial phase-lock loop (SPECS) [40,41]. MFM tips were prepared by depositing a nominally 100-nm-thick Co film onto bare tips using electron-beam evaporation. A ~ 50 -nm-thick Au film was deposited on the surface of the h -LuFeO₃ film to eliminate electrostatic interaction between the sample and the magnetic tip. The MFM images were taken in a noncontact mode with a scanning plane ~ 40 nm above the sample surface. The MFM signal, i.e., the change

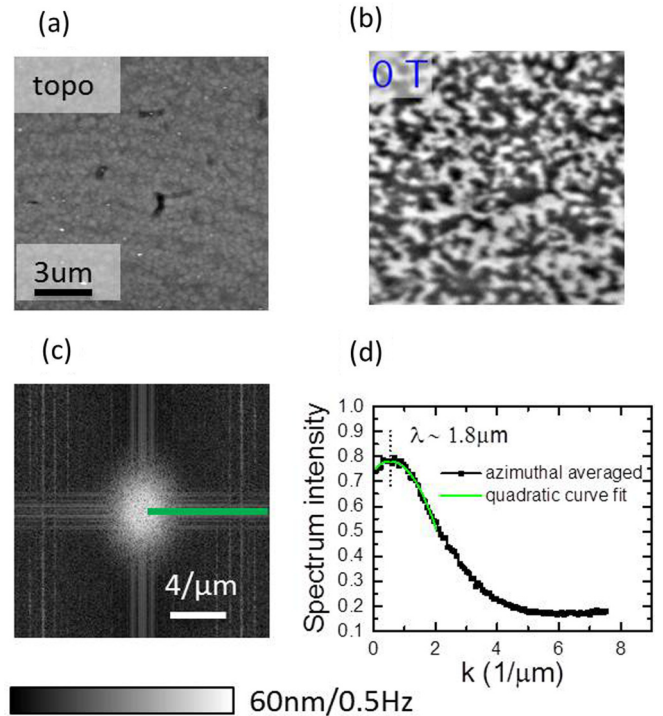


FIG. 2. (a) Topographic and (b) MFM image of the h -LuFeO₃ film at 50 K after zero-field cooling. (c) Fourier transformation (FT) image of (b); the virgin domain state shows a ringlike feature at the center. (d) k dependence of radial FT spectrum intensity (azimuthally averaged) shows a single peak at $\lambda \sim 1.8 \mu\text{m}$. The green curve is the quadratic curve fit around the peak.

of the cantilever resonant frequency, is proportional to the out-of-plane stray field gradient [42]. Dark (bright) regions in MFM images represent more (less) attractive interaction between the film and the magnetic tip. The magnetoelectric force microscopy (MeFM) measurement was conducted by applying a modulated voltage to the bottom electrode of the sample and using a lock-in amplifier to demodulate the MFM signals [23,43]. The bottom electrode was a layer of silver epoxy glued on the backside of the 100- μm -thick YSZ (111) substrate.

III. RESULTS AND DISCUSSION

Figure 2 shows the topographic and MFM images of the h -LuFeO₃ film at 50 K after zero-field cooling (ZFC). The topographic image shows a flat, Au-capped surface with a roughness ~ 3.5 nm. As shown in Fig. 2(b), a labyrinthlike domain structure was observed in the virgin domain state, which is typical for thin films of uniaxial ferromagnets [44,45]. The characteristic domain size of h -LuFeO₃ is estimated by Fourier transform (FT) analysis of the virgin domain state, as shown in Fig. 2(c). The image shows a ringlike feature in the center, indicating an isotropic domain size distribution. The azimuthally averaged FT spectral intensity as a function of wave vector k is shown in Fig. 2(d), which exhibits one broad peak slightly above zero. Using a quadratic fit, the peak was found at $\lambda \sim 1.8 \mu\text{m}$, which is the characteristic domain size of the 200-nm-thick h -LuFeO₃

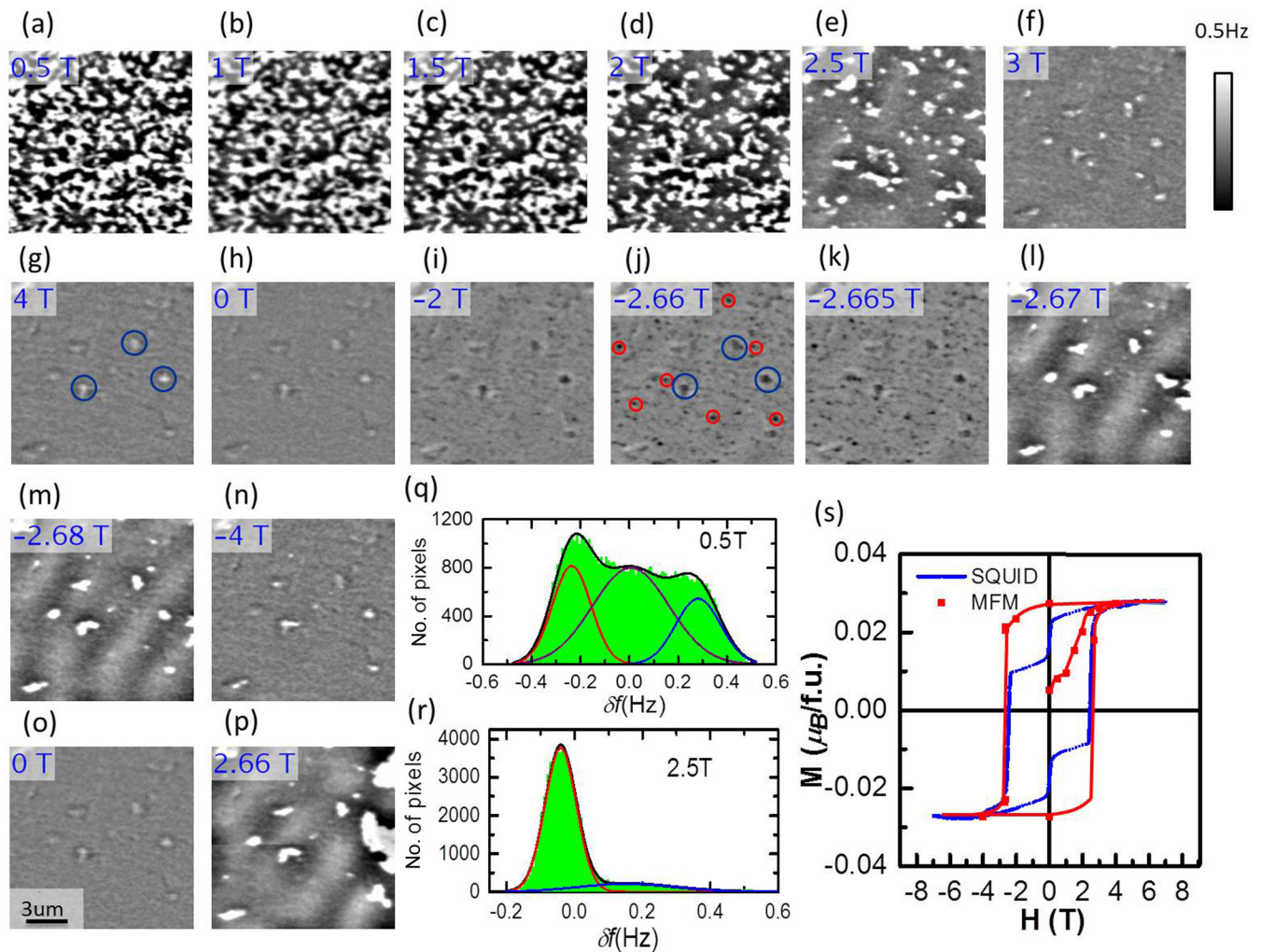


FIG. 3. (a)–(p) MFM images (50 K) taken at various magnetic fields after zero-field cooling. The zero-field MFM image is shown in Fig. 2(b). The magnetic field value of each image is labeled at the top left corner. The gray scale of the MFM images is 0.5 Hz. Representative defect sites and nucleation sites are labeled by blue and red circles, respectively. Histograms of the MFM images at (q) 0.5 T and (r) 2.5 T reveal multiple peaks. The profiles can be fit by a combination of either (q) three or (r) two Gaussian peaks. The bin's number was set to be 100. (s) M-H curves measured by SQUID (blue) and MFM (red) show $H_c \sim 2.66$ T (50 K).

film after ZFC. The apparently random domain configuration indicates a significant amount of nucleation and pinning sites. To characterize these properties, the magnetization saturation and reversal process are visualized with MFM.

Figure 3 shows the evolution of the weak ferromagnetic domains as a function of the external magnetic field. The zero-field MFM image is shown in Fig. 2(b). A magnetic field of 0.5 T is not strong enough to modify the domain pattern, as shown in Fig. 3(a). The domain contrast was enhanced ~ 1.8 times, likely due to the enhancement of the MFM tip moment. Further increasing the field results in a gradual reduction of the antiparallel domains due to depinning of the domain boundaries. As shown in Figs. 3(b)–3(g), the dark regions expand and the bright regions shrink with increasing external magnetic field. The film saturates at 4 T because a further increase of the external magnetic field does not cause any change of the domain pattern. Note that some weak domain contrast is still visible in the saturated state. Those features are not correlated with topography. So they

are magnetic defects (labeled by blue circles), likely due to local structural or composition imperfections. The film stays in the saturated state even after the field is ramped down to zero, as shown in Fig. 3(h). The domain contrast is reversed at -2 T, indicating the tip moment was switched. This also verifies that the domain contrast observed in the saturated state is magnetic. On the other hand, no reversed domain was found in the scanned area. Maintaining a single domain state under reverse field is a telltale sign of a strong uniaxial anisotropy in h -LuFeO₃, which prevents nucleation of reversed domains. At -2.66 T, many bubblelike reversed domains (labeled by red circles) were observed in the MFM image, as shown in Fig. 3(j). This confirms a relatively dense concentration of nucleation sites randomly distributed over the film. Further decreasing the magnetic field by 5 mT induces little change in the domain pattern. From -2.665 to -2.670 T, the domain pattern changes dramatically. At -2.67 T, the film is dominated by down domains with only a small amount of up domains (bright contrast) pinned by defect sites. The sharp transition

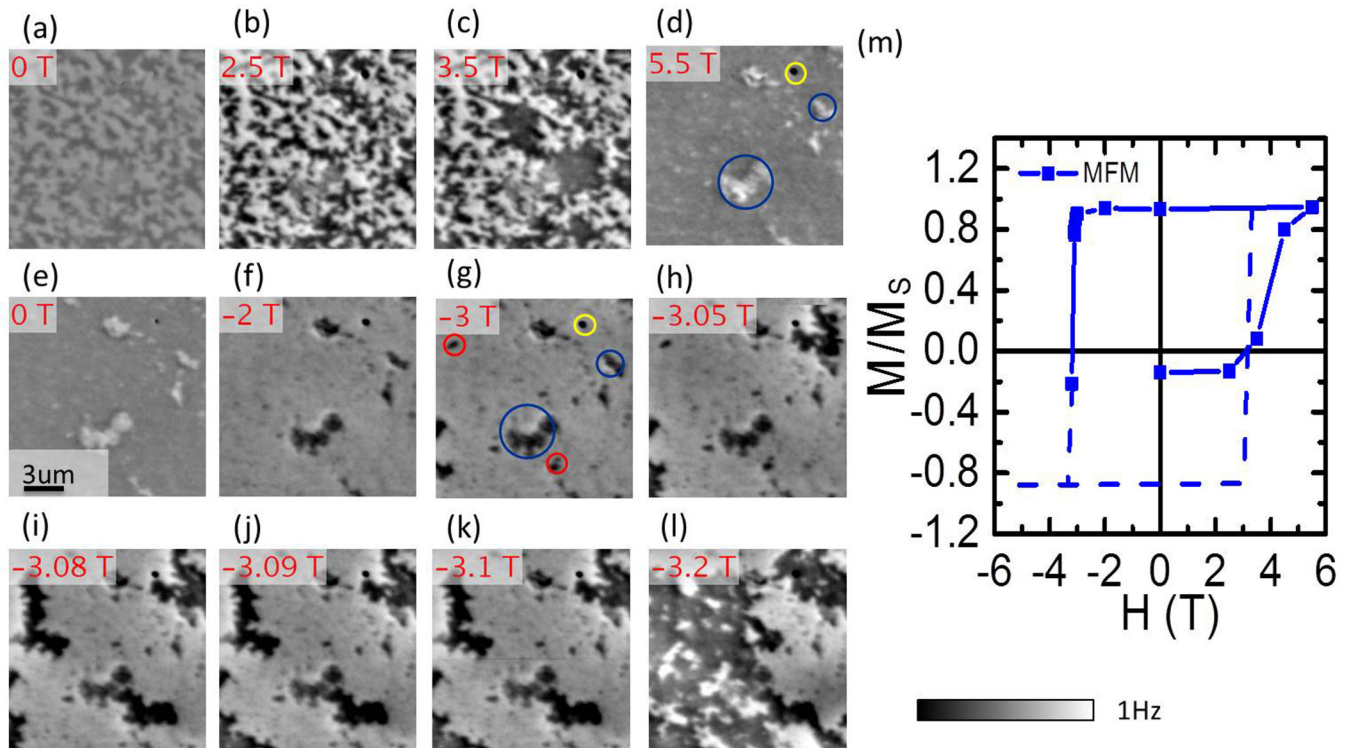


FIG. 4. (a)–(l) MFM images (6 K) of the h -LuFeO₃ film measured at various magnetic fields after ZFC. The gray scale is 1 Hz. Representative defect sites, nucleation sites, and topographic features are labeled by blue, red, and yellow circles, respectively. (m) M - H curve deduced from the MFM images reveals a stronger pinning effect of a hard ferromagnet at 5 K, with $H_C \sim 3.2$ T. Note that the dashed line is replicated from measured results via symmetry.

from a positive-magnetization to negative-magnetization state suggests a relatively narrow distribution of domain wall pinning strength at 50 K. Further decreasing the magnetic field to -4 T aligned all of the magnetic domains, i.e., the film was saturated, showing identical features as the positively saturated state, further corroborating that they are magnetic defects. Interestingly, a similar domain pattern was observed at positive coercive field H_C , as shown in Fig. 3(p), which indicates a strong memory effect.

A histogram analysis was also carried out on these field-dependent MFM images (256×256 pixels) to estimate the population of up and down domains. The histogram curves of a near-zero magnetization multidomain state [Figs. 3(a)–3(d)] can be fitted by a superposition of three Gaussian peaks, as shown in Fig. 3(q). Left (red curve) and right (blue curve) peaks correspond to up and down weak ferromagnetic domains. The middle peak (purple curve) may originate from the domain wall contributions. The histogram profiles of the polarized domain states (e.g., 2.5 T), however, exhibit a two-peak feature due to a reduced contribution from domain walls. We used the peak height to estimate the population of up and down domains. The normalized magnetization M/M_S therefore can be estimated from $(N_\uparrow - N_\downarrow)/(N_\uparrow + N_\downarrow)$, where M_S is the saturation magnetization and N_\uparrow (N_\downarrow) is the population of up (down) domains. From the normalized magnetization, the M vs H loop (red curve) can be plotted from the MFM images. It shows a squarelike hysteresis loop of a hard ferromagnet with a strong uniaxial anisotropy. The virgin curve shows that domain walls start to depin at ~ 1.5 T, much lower than

the coercive field. This indicates a relatively wider pinning strength distribution of the virgin domain state at 50 K. In contrast, the sharp transition at the coercive field suggests that the nucleation sites are also strongly pinning. The M - H data from a superconducting quantum interference device (SQUID) measurement (blue curve) on the same film shows a two-step behavior. The first step at zero field, which is absent in the MFM data, is likely coming from a small amount of iron-rich impurity phase (e.g., Fe₃O₄). The second step at $H_C \sim 2.660$ T is in good agreement with that inferred from our MFM data. This provides compelling evidence that our MFM observation reflects the representative domain behavior of the h -LuFeO₃ thin films grown by MBE.

Although the SQUID data at 50 K has been confirmed by MFM measurements, the characterization of the weak ferromagnetism at lower temperature is still lacking. The SQUID measurement of h -LuFeO₃ below 50 K is challenging because the substantial paramagnetic background of the YSZ substrate dominates the magnetization signals. MFM signal, however, is not sensitive to uniform magnetization (e.g., paramagnetic background). Thus, MFM is a suitable technique to study the weak ferromagnetism of h -LuFeO₃ at low temperature [46]. Figure 4 shows the field-dependent MFM measurements at a different location at 6 K after ZFC. A similar labyrinthlike virgin domain state was observed, confirming that our MFM (local) observation is representative. The virgin domain state persists up to 2.5 T, indicating a stronger domain wall pinning effect. The domain walls start to propagate at 3.5 T, a much higher applied magnetic field than that needed at 50 K.

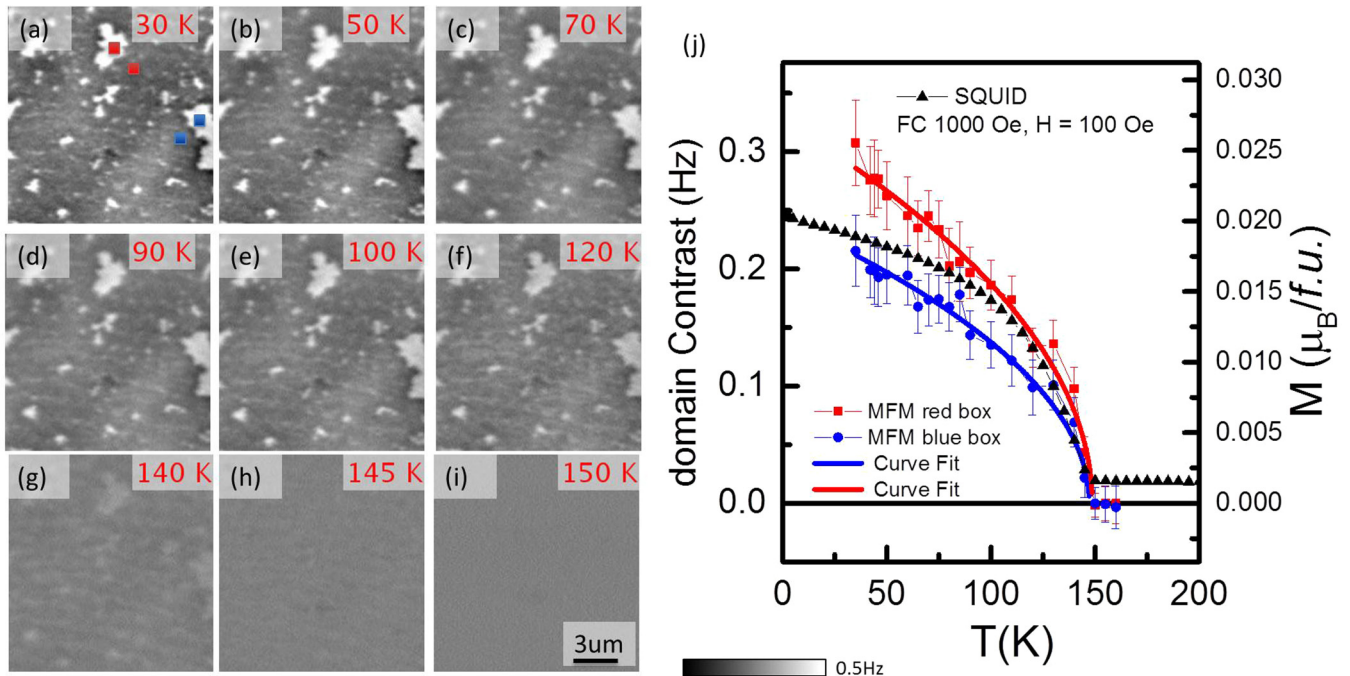


FIG. 5. (a)–(i) Zero-field MFM images of induced weak ferromagnetic domains measured at various temperature. (j) Temperature dependence of domain contrast from MFM images (red and blue boxes) is consistent with that of magnetization measured by SQUID (black triangles), indicating a second-order ferromagnetic transition at $T_C \approx 147$ K. It can be fitted by a mean-field-like behavior (blue and red curves).

The film saturates at 5.5 T. The saturated state shows a higher concentration of magnetic defects than the previously measured region at 50 K. The dark dot (labeled by a yellow circle) comes from a high topographic feature. The film stays in the saturation state as the field is ramped down to zero and negative fields. At -2 T, the domain contrast of the magnetic defects is reversed, indicating a reversal of the MFM tip moment. The topographic feature, however, is still attractive, confirming its nonmagnetic origin. Down domains start to nucleate at ~ -3 T. As shown in Fig. 4(g), fewer nucleation sites can be identified, in contrast to the 50 K case. From -3 and -3.2 T, the MFM results reveal clear domain reversal behavior via domain nucleation and domain wall propagation, as shown in Figs. 4(g)–4(l). The down domains tend to nucleate from the defect sites, suggesting a lower nucleation energy barrier at these regions. In contrast to 50 K data, the magnetic transition at 6 K is much smoother, indicating a stronger domain wall pinning effect. This facilitates the MFM imaging of the intermediate multidomain states. At $H_C \sim -3.2$ T, the concentration of up and down domains is approximately equal. The M - H loop at 6 K can be deduced by using the aforementioned histogram analysis. In contrast to the 50 K data, the virgin curve at 6 K data exhibits a pinning-dominated behavior. This is likely due to collective pinning from a high density of strong pinning sites.

The strong pinning preserves the domain configuration to high temperature. This enables an investigation of the temperature dependence of the magnetization via MFM domain contrast. The temperature dependence of the pinned weak ferromagnetic domains is shown in Figs. 5(a)–5(i). As the temperature increases, the domain contrast becomes

weaker and weaker. At 150 K, the domain contrast disappears, indicating a phase transition from a weak ferromagnetic state to a paramagnetic state. The temperature dependence of the domain contrast exhibits a mean-field-like behavior, as shown in Fig. 5(j), which can be fitted by $M = A(T_C - T)^{0.5}$. The fitting results give the $T_C \sim 148$ K and $M_S \sim 0.242$ Hz. The M - T curve from SQUID shows $T_C \approx 147$ K, in good agreement with MFM data, and $M_S \sim 0.02 \mu_B/\text{f.u.}$, which can be used as a good calibration of our MFM data. The conversion factor between magnetization M and MFM data is $0.0826 \mu_B/\text{f.u.}/\text{Hz}$. Given the ~ 21 mHz noise level of our MFM system, the sensitivity limit of our setup to probe magnetic moments in this 200 nm thin film is $0.002 \mu_B/\text{f.u.}$ (i.e., 1-nm-thick film would be $0.4 \mu_B/\text{f.u.}$).

The MeFM measurement has also been performed on a h -LuFeO₃ film with multidomain structures. Assuming the film stays in the single ferroelectric domain state at low temperature, the ME domains should be coupled with weak ferromagnetic domains. Unfortunately, we did not observe any ME signals. One possible explanation is that the weak ME effect is below our detection limit, assuming the polarization domains (if any) do not change during the magnetization reversals. Considering the ~ 1 mHz noise level of our MeFM, the smallest magnetization change we can measure is $\delta M = 1.38 \times 10^{-6} \mu_B/\text{\AA}^3$. The dielectric constants of YSZ and h -LuFeO₃ film are 27 and 20, respectively [35,47]. The maximum electric field applied on the h -LuFeO₃ film is approximately 2.7×10^6 V/m using a simple double-dielectric layer model. Therefore, the ME sensitivity of our MeFM is ~ 6.0 ps/m, which is more than an order of magnitude larger than the theoretically predicted value of ~ 0.16 ps/m. In order

to observe the weak ME effect, we need to improve the MeFM sensitivity. One possible route is to use a MFM tip with larger magnetic moment. Another one is to enhance the electric field by thinning down the YSZ substrate or growing epitaxial Pt bottom electrode. Current leakage due to pin holes in thin films may, however, limit the application of high electric fields.

IV. CONCLUSION

In conclusion, we present a systematic study of the domain behavior in thin films of the weak ferromagnet h -LuFeO₃ using cryogenic MFM. Isotropic labyrinthlike weak ferromagnetic domain patterns with a size of $\sim 1.8 \mu\text{m}$ are observed below $T_C \sim 147 \text{ K}$ after ZFC. At low temperature (6 K), the film behaves like a typical pinning-dominated hard ferromagnet. At elevated temperature (50 K), the domain nucleation sites become denser and the domain wall pinning effect is suppressed, which is consistent with the general scenario of thermally activated domain nucleation and domain wall depinning. Our MFM setup has a high sensitivity to probe

small canted moments ($\sim 0.002 \mu_B/f.u.$) with a reasonably good signal-to-noise ratio. This technique is promising to investigate materials with small magnetic moments, such as weak ferromagnets and diluted magnetic semiconductors.

ACKNOWLEDGEMENTS

This work at Rutgers University is supported by the office of Basic Energy Science, Division of Materials Sciences and Engineering, US Department of Energy Award No. DE-SC0008147. Research at Cornell University was primarily supported by the US Department of Energy, Office of Basic Energy Sciences, Division of Materials Sciences and Engineering, under Award No. DE-SC0002334. Substrate preparation was performed in part at the Cornell NanoScale Facility, a member of the National Nanotechnology Coordinated Infrastructure (NNCI), which is supported by the National Science Foundation (Grant No. ECCS-15420819). Electron microscopy facilities supported by the Cornell Center for Materials Research, through the National Science Foundation (Grants No. DMR 1120296 and No. 1429155).

-
- [1] N. A. Spaldin and M. Fiebig, *Science* **309**, 391 (2005).
 [2] W. Eerenstein, N. D. Mathur, and J. F. Scott, *Nature (London)* **442**, 759 (2006).
 [3] R. Ramesh and N. A. Spaldin, *Nat. Mater.* **6**, 21 (2007).
 [4] S. Dong, J. M. Liu, S. W. Cheong, and Z. F. Ren, *Adv. Phys.* **64**, 519 (2015).
 [5] M. Fiebig, *J. Phys. D: Appl. Phys.* **38**, R123 (2005).
 [6] J. P. Rivera, *Eur. Phys. J. B* **71**, 299 (2009).
 [7] K. F. Wang, J. M. Liu, and Z. F. Ren, *Adv. Phys.* **58**, 321 (2009).
 [8] M. Bibes and A. Barthelemy, *Nat. Mater.* **7**, 425 (2008).
 [9] N. Hur, S. Park, P. A. Sharma, J. S. Ahn, S. Guha, and S. W. Cheong, *Nature (London)* **429**, 392 (2004).
 [10] S. Dong, J. Zhai, F. Bai, J. F. Li, and D. Viehland, *Appl. Phys. Lett.* **87**, 062502 (2005).
 [11] J. Ryu, S. Priya, K. Uchino, and H. E. Kim, *J. Electroceram.* **8**, 107 (2002).
 [12] S. Shastry, G. Srinivasan, M. I. Bichurin, V. M. Petrov, and A. S. Tatarenko, *Phys. Rev. B* **70**, 064416 (2004).
 [13] A. S. Tatarenko, V. Gheevarghese, and G. Srinivasan, *Electron. Lett.* **42**, 540 (2006).
 [14] G. A. Smolenskiĭ and I. E. Chupis, *Sov. Phys. Usp.* **25**, 475 (1982).
 [15] J. Wang, J. B. Neaton, H. Zheng, V. Nagarajan, S. B. Ogale, B. Liu, D. Viehland, V. Vaithyanathan, D. G. Schlom, U. V. Waghmare, N. A. Spaldin, K. M. Rabe, M. Wuttig, and R. Ramesh, *Science* **299**, 1719 (2003).
 [16] C. Ederer and C. J. Fennie, *J. Phys.: Condens. Matter* **20**, 434219 (2008).
 [17] C. J. Fennie, *Phys. Rev. Lett.* **100**, 167203 (2008).
 [18] G. Catalan and J. F. Scott, *Adv. Mater.* **21**, 2463 (2009).
 [19] T. Katsufuji, S. Mori, M. Masaki, Y. Moritomo, N. Yamamoto, and H. Takagi, *Phys. Rev. B* **64**, 104419 (2001).
 [20] M. Fiebig, T. Lottermoser, D. Frohlich, A. V. Goltsev, and R. V. Pisarev, *Nature (London)* **419**, 818 (2002).
 [21] B. B. V. Aken, T. T. M. Palstra, A. Filippetti, and N. A. Spaldin, *Nat. Mater.* **3**, 164 (2004).
 [22] F. Yen, C. dela Cruz, B. Lorenz, E. Galstyan, Y. Y. Sun, M. Gospodinov, and C. W. Chu, *J. Mater. Res.* **22**, 2163 (2007).
 [23] Y. Geng, H. Das, A. L. Wysocki, X. Wang, S. W. Cheong, M. Mostovoy, C. J. Fennie, and W. Wu, *Nat. Mater.* **13**, 163 (2014).
 [24] A. R. Akbashev, A. S. Semisalova, N. S. Perov, and A. R. Kaul, *Appl. Phys. Lett.* **99**, 122502 (2011).
 [25] Y. K. Jeong, J.-H. Lee, S.-J. Ahn, and H. M. Jang, *Chem. Mater.* **24**, 2426 (2012).
 [26] H. Iida, T. Koizumi, Y. Uesu, K. Kohn, N. Ikeda, S. Mori, R. Haumont, P. E. Janolin, J. M. Kiat, M. Fukunaga, and Y. Noda, *J. Phys. Soc. Jpn.* **81**, 024719 (2012).
 [27] W. B. Wang, J. Zhao, W. B. Wang, Z. Gai, N. Balke, M. F. Chi, H. N. Lee, W. Tian, L. Y. Zhu, X. M. Cheng, D. J. Keavney, J. Y. Yi, T. Z. Ward, P. C. Snijders, H. M. Christen, W. D. Wu, J. Shen, and X. S. Xu, *Phys. Rev. Lett.* **110**, 237601 (2013).
 [28] J. A. Moyer, R. Misra, J. A. Mundy, C. M. Brooks, J. T. Heron, D. A. Muller, D. G. Schlom, and P. Schiffer, *APL Mater.* **2**, 012106 (2014).
 [29] X. S. Xu and W. B. Wang, *Mod. Phys. Lett. B* **28**, 1430008 (2014).
 [30] S. M. Disseler, J. A. Borchers, C. M. Brooks, J. A. Mundy, J. A. Moyer, D. A. Hillsberry, E. L. Thies, D. A. Tenne, J. Heron, M. E. Holtz, J. D. Clarkson, G. M. Stiehl, P. Schiffer, D. A. Muller, D. G. Schlom, and W. D. Ratcliff, *Phys. Rev. Lett.* **114**, 217602 (2015).
 [31] H. Das, A. L. Wysocki, Y. N. Geng, W. D. Wu, and C. J. Fennie, *Nat. Commun.* **5**, 2998 (2014).
 [32] E. Magome, C. Moriyoshi, Y. Kuroiwa, A. Masuno, and H. Inoue, *Jpn. J. Appl. Phys.* **49**, 09ME06 (2010).
 [33] A. Masuno, A. Ishimoto, C. Moriyoshi, N. Hayashi, H. Kawaji, Y. Kuroiwa, and H. Inoue, *Inorg. Chem.* **52**, 11889 (2013).
 [34] S. M. Disseler, X. Luo, B. Gao, Y. S. Oh, R. W. Hu, Y. Z. Wang, D. Quintana, A. Zhang, Q. Z. Huang, J. N. Lau, R. Paul, J. W.

- Lynn, S. W. Cheong, and W. Ratcliff, *Phys. Rev. B* **92**, 054435 (2015).
- [35] L. Lin, H. M. Zhang, M. F. Liu, S. Shen, S. Zhou, D. Li, X. Wang, Z. B. Yan, Z. D. Zhang, J. Zhao, S. Dong, and J.-M. Liu, *Phys. Rev. B* **93**, 075146 (2016).
- [36] A. A. Bossak, I. E. Graboy, O. Y. Gorbenko, A. R. Kaul, M. S. Kartavtseva, V. L. Svetchnikov, and H. W. Zandbergen, *Chem. Mater.* **16**, 1751 (2004).
- [37] J. A. Mundy, C. M. Brooks, M. E. Holtz, J. A. Moyer, H. Das, A. F. Rebola, J. T. Heron, J. D. Clarkson, S. M. Disseler, Z. Q. Liu, A. Farhan, R. Held, R. Hovden, E. Padgett, Q. Y. Mao, H. Paik, R. Misra, L. F. Kourkoutis, E. Arenholz, A. Scholl, J. A. Borchers, W. D. Ratcliff, R. Ramesh, C. J. Fennie, P. Schiffer, D. A. Muller, and D. G. Schlom, *Nature (London)* **537**, 523 (2016).
- [38] W. Wang, Y. Geng, and W. Wu, *Appl. Phys. Lett.* **104**, 072905 (2014).
- [39] W. Wang, Y. Sun, Y. Zhao, and W. Wu, *Appl. Phys. Lett.* **108**, 122901 (2016).
- [40] W. Wang, F. Yang, C. Gao, J. Jia, G. D. Gu, and W. Wu, *APL Mater.* **3**, 083301 (2015).
- [41] W. Wang, C.-Z. Chang, J. S. Moodera, and W. Wu, *npj Quantum Mater.* **1**, 16023 (2016).
- [42] D. Rugar, H. J. Mamin, P. Guethner, S. E. Lambert, J. E. Stern, I. McFadyen, and T. Yogi, *J. Appl. Phys.* **68**, 1169 (1990).
- [43] Y. Geng and W. Wu, *Rev. Sci. Instrum.* **85**, 053901 (2014).
- [44] V. Gehanno, A. Marty, B. Gilles, and Y. Samson, *Phys. Rev. B* **55**, 12552 (1997).
- [45] A. Hubert and R. Schafer, *Magnetic Domains* (Springer, Berlin, 1998).
- [46] Y. N. Geng, J. H. Lee, D. G. Schlom, J. W. Freeland, and W. D. Wu, *Phys. Rev. B* **87**, 121109 (2013).
- [47] http://www.mtixtl.com/ysz1002diax05mm2sp_1-1-2.aspx (unpublished).